

Characteristics of Sand Transport on the Surface of Transverse Ridge Microtopography

Wenru Jia¹, Xiuming Li¹, Qing Li², Haiming Yan¹, Baoni Xie¹, and Hao Wei¹

¹Hebei GEO University

²Hebei Academy of Sciences

July 6, 2022

Abstract

Through wind tunnel experiments, we measured the surface drifting sand flux structure and sand transport rate at height of 0~70 cm on a bed surface under conditions of ridge microtopography with different height and different spacing. The results show that the percentage of sand transport in 0~10 cm layer above the bed surface is significantly reduced under ridge microtopography condition compared with no ridges condition. Under ridge microtopography condition, the percentage of sand transport in 0~10 cm layer decreases with the increase of ridge height, while it generally increases with the increase of ridge spacing and wind velocity. Under no ridges condition, the sand transport rate decreases in a power function law with the increase of height. The variation of sand transport rate with height under ridge microtopography condition could be divided into two cases: one shows that sand transport rate decreases exponentially with the increase of height, while the other shows that sand transport rate increases with the increase of height under a certain height, and above the certain height it decreases exponentially with the increase of height, known as “elephant nose” effect which seems similar to the structure of drifting sand flux in Gobi desert. For all the ridge heights and spacings, the total sand transport rate at height of 0~70 cm increases with the increase of friction velocity in a power function law, and it increases with the increase of ridge spacing. The simulation of the drifting sand flux structure and the relationship between sand transport rate and height shows that the ridge microtopography reduces the sand transport ratio of near surface air flow compared with no ridges condition. The results will contribute to studies on recognizing the process and mechanism of soil wind erosion in ridge farmland.

Characteristics of Sand Transport on the Surface of Transverse Ridge Microtopography

Authors: Wenru Jia^{1,2}, Xiuming Li^{3*}, Qing Li⁴, Haiming Yan^{1,2}, Baoni Xie^{1,2}, Hao Wei²

1. *School of Land Science and Space Planning, Hebei GEO University, No. 136 East Huai'an Road, Shijiazhuang 050031, China*

2. *Natural Resource Asset Capital Research Center, Hebei GEO University, Shijiazhuang 050031, China*

3. *School of Management, Hebei GEO University, No. 136 East Huai'an Road, Shijiazhuang 050031, China*

4. *Institute of Geographical Sciences, Hebei Academy Sciences, Hebei Engineering Research Center for Geographic Information Application; Shijiazhuang Hebei, 050011, China*

***Corresponding author:** Xiuming Li, Email:

lixiuming010@163.com

Tel./Fax: +86 311 8720 7673

ABSTRACT

Through wind tunnel experiments, we measured the surface drifting sand flux structure and sand transport rate at height of 0~70 cm on a bed surface under conditions of ridge microtopography with different height and different spacing. The results show that the percentage of sand transport in 0~10 cm layer above the bed surface is significantly reduced under ridge microtopography condition compared with no ridges condition. Under ridge microtopography condition, the percentage of sand transport in 0~10 cm layer decreases with the increase of ridge height, while it generally increases with the increase of ridge spacing and wind velocity. Under no ridges condition, the sand transport rate decreases in a power function law with the increase of height. The variation of sand transport rate with height under ridge microtopography condition could be divided into two cases: one shows that sand transport rate decreases exponentially with the increase of height, while the other shows that sand transport rate increases with the increase of height under a certain height, and above the certain height it decreases exponentially with the increase of height, known as "elephant nose" effect which seems similar to the structure of drifting sand flux in Gobi desert. For all the ridge heights and spacings, the total sand transport rate at height of 0~70 cm increases with the increase of friction velocity in a power function law, and it increases with the increase of ridge spacing. The simulation of the drifting sand flux structure and the relationship between sand transport rate and height shows that the ridge microtopography reduces the sand transport ratio of near surface air flow compared with no ridges condition. The results will contribute to studies on recognizing the process and mechanism of soil wind erosion in ridge farmland.

Key words :Wind tunnel experiments; ridge microtopography; drifting sand flux structure; sand transport rate; friction velocity

INTRODUCTION

Sand transport rate is a measure of the capacity of transporting sand particles by wind. It is the amount of sand carried by the air flow through the unit width in unit time, also known as the solid flow of drifting sand flux (Lancaster et al., 1996; Zhao et al., 2021). There are many factors affecting the sand transport rate, including wind force, density, particle size, specific gravity and shape of sand, as well as moisture rate of sand, earth surface features and atmosphere stability (Kok et al., 2012; Miao et al., 2012; Avezilla et al., 2017; Favaro et al., 2020).

The study of drifting sand flux originated with Bagnold's research on the physics of blown sand and desert dunes (Bagnold, 1941). Exner obtained the distribution of sand transport rate with elevation according to the diffusion theory (Wu, 2003). Horikawa (1982) regarded the phenomenon of wind-blown sand as a group movement of sand particles, made statistical treatment, and put forward the theory of sand density distribution and sand transport rate distribution with height in the sand transport layer. Znamenski (Ding, 2010) studied the relationship between the structural characteristics of drifting sand flux and sand wind erosion and accumulation through wind tunnel experiments and field observations, and he used the structure number of drifting sand flux (Q_{max}/Q) to describe the structure of drifting sand flux, which was used as the basis for judging the process of wind erosion. Ma et al. (1987) put forward the three laws of the structure of drifting sand flux according to the research of domestic and international scholars. Wu Zheng (2003) proposed using the characteristic value λ of drifting sand flux structure to measure the variation characteristics of surface erosion and deposition. Fryear and Saleh (1993) put forward the distribution function of drifting sand flux with height according to the long-term observation and research of soil wind erosion research station in Big Spring, Texas, USA. They believe that the variation of saltation sand transport with height follows the distribution law of power function, while the suspended sediment follows the distribution law of exponential function. The study on the structure of drifting sand flux on different underlying surfaces shows that the distribution of sand transport rate on the sand surface with vertical height basically satisfies the exponential function (Ha, 2004; Zhang et al., 2022). There is a turning height of Gobi drifting sand flux on the sand bed. Below this height, the sand transport rate increases with the increase of height, and beyond this height, the sand transport rate decreases with the increase of height. The distribution characteristics of this drifting sand flux structure are vividly called "elephant nose" effect (Qu et al., 2005; Zhang et al., 2007).

The type of underlying surface affects the turbulence of near surface airflow. Therefore, for a specific type of underlying surface, there is a unique structure model of drifting sand flux. Ridge microtopography increases the surface fluctuation and enhances the turbulence of near surface airflow, which changes the spatial distribution of sand-carrying airflow energy, and then changes the structure of near surface drifting sand flux. This paper intends to explore the variation law of drifting sand flux structure and sand transport rate under the condition of ridge microtopography by studying the drifting sand flux structure and sand transport rate under different ridge microtopography conditions.

RESEARCH METHODS

2.1 Wind tunnel experiments

The experiments were carried out in a straight line forced wind tunnel of the State Key Laboratory of Earth Surface Processes and Resource Ecology, Beijing Normal University. The total length of the wind tunnel is 71.1 m, and the experimental section is 24 m long, 3 m wide, and 2 m tall, and the experimental axial wind velocity is continuously adjustable from 2 to 45 m·s⁻¹. Details are provided by Cheng et al. (2015).

2.2 Experimental design

The ridge models are made of wood, and the section is a right angle isosceles triangle. The soil sample is a sandy soil in Zhenglan Banner, Inner Mongolia, in northern China, and its grain-size composition of the soil was provided by (Jia et al., 2019). The sand sampler used in the experiments is a special sand sampler for wind tunnel developed and produced by the MOE Engineering Research Center of Desertification and Blown-sand Control of Beijing Normal University, which is composed by a bracket and seven sand collecting boxes, with a height of 70 cm, and the cross-sectional area of each sand inlet is 10 cm × 10 cm. The sand flow within the height range of 70 cm above the bed surface can be collected. The sand collecting boxes are rectangular, sealed at the bottom, wedge-shaped at the opening end, stainless steel on three sides and mesh one side, which serves as an exhaust port to discharge the air flow in sand collecting boxes. The inlet end of the sand collection box is designed to be wedge-shaped, which can effectively relieve the blocking airflow at the inlet and effectively improve the sand collection efficiency (Fig.1). The experimental wind velocity is 70 cm high axis wind velocity, which is measured by "L" pitot tube. They are 8, 10, 12, 14 and 16 m·s⁻¹ respectively, and the corresponding friction velocities (u_*) are 0.34, 0.42, 0.51, 0.59 and 0.68 m·s⁻¹ respectively. 25 ridge structures and a control one with no ridges were designed in the simulation experiments, including 5 ridge heights (H=5, 7.5, 10, 12.5 and 15 cm) and 5 ridge spacings (L=5H, 10H, 15H, 20H, and 25H).

2.3 Experimental methods

In wind erosion experiments, soil samples were spread in a whole sample trough which is 1 m wide, 10 m long, and 3~5 cm deep. Soil surface was smoothed and then the ridge models were laid on it. The sand sampler was arranged at the end of the sample trough to collect sand mass at different heights (Fig.2). After each blowing experiments, the sand collecting boxes were taken out one by one, and the sand mass was measured by an electronic balance to calculate the structure of drifting sand flux and sand transport rate. The observation time varies according to the ridge spacing and the experimental wind velocity. The observation time of each ridge spacing is shown in table 1.

RESULTS AND ANALYSIS

3.1 Structure of drifting sand flux with no ridges

Under the condition of no ridges, the sand transport rate at height of 0~70 cm above the sand bed decreases with the increase of height and continues to increase with the increase of friction velocity (Table 2). More than 97% of the sand transport is concentrated at height of 0~10 cm, and the sand transport decreases rapidly in 10~20 cm layer, accounting for 1.59% of the total sand transport on average. With the increase of height, the sand transport decreases gradually, but the decreasing rate between layers is getting smaller and smaller, and the sand transport in each layer above 20 cm is no more than 1%. With the increase of friction

velocity, the proportion of sand transported in the drifting sand flux layer near the bed decreases relatively, and the proportion of sand transported in the upper layer increases accordingly. Based on the measurement results of sand transport, the sand transport rate at each height level (the average values of upper and lower heights are taken for each height level) is calculated (Fig. 3), and the correlation between the sand transport rate and height is analyzed. The results show that the sand transport rate decreases with the increase of height in a power function, which can be expressed by the function $q = Ah^{-B}$, and the correlation coefficients are all above 0.941.

3.2 Drifting sand flux Structures with microtopography of ridges

The features of underlying surface and wind velocity are the main factors affecting the drifting sand flux (Lancaster et al., 1998; Butterfield, 1999). The fluctuation of underlying surface changes the saltation trajectory of sand particles (Anderson and Hallet, 1986; Tsoar and White, 1996; Frank and Kocurek, 1996; Wiggs, 2001), while the change of wind velocity changes the movement properties of sand particles in the drifting sand flux, which eventually leads to the change of the drifting sand flux structure (Huang and Zheng, 2007). The experimental results show that the total sand transport rate at 0~70 cm height with different ridges increases continuously with the increase of wind velocity, but the change of sand transport rate with height can be divided into two cases. One is that the sand transport rate decreases with the increase of height, and the fitting relationship between surface sand transport rate and height deviates from the power function law with no ridges, but mostly obeys the exponential function law of particle distribution of reaction saltation. The other is that the sand transport rate increases with the increase of height below a certain height, and decreases with the increase of height above the certain height, showing the "elephant nose" effect similar to drifting sand flux structure in Gobi desert. The distribution of the sand transport rate with ridges under different heights can be divided into two sections, the lower section has no obvious law, and the upper section still follows the exponential function law (Fig. 4).

Mostly, the variation of sand transport rate with ridge structures (the combination of height and spacing) changing with height near surface conforms to the first case. The sand transport rate is largest in 0~10 cm layer, but the percentage of sand transport is significantly lower than that with no ridges. The sand transport rate decreases rapidly in 10~20 cm layer, while the decreasing rate of sand transport rate above 20 cm height goes smaller. Taking a ridge height of 5 cm as an example (Table 3), the sand transport rate of 0~10 cm layer accounts for 58.38% of the total sand transport rate, 10~20 cm layer rapidly decreases to 21.24%, 20~60 cm layer keeps decreasing with a smaller reducing rate, and in 60~70 cm layer, the sand transport rate decreases to 1.96%. Compared with the condition with no ridges, the sand transport rate under different ridge structures decreases obviously in 0~10 cm layer, while increases significantly in 20~60 cm layer, and increases slightly in the uppermost layer. The maximum height of sand saltation also increases accordingly. Only when the friction velocity is small, except for a few ridge structures, the sand saltation reaches the maximum height within 70 cm height, the others do not reach the maximum height.

The surface sand transport rate of some ridge structures conforms to the second case, and the higher the ridge height is, the more common this phenomenon is. Taking a ridge height of 15 cm and a ridge spacing of 15H as an example, when the friction velocity is $0.68 \text{ m}\cdot\text{s}^{-1}$ and the height layer increases from 0~10 cm to 30~40 cm, the sand transport rate continuously increases from $0.0742 \text{ g}\cdot\text{cm}^{-2}\cdot\text{min}^{-1}$ to $0.2284 \text{ g}\cdot\text{cm}^{-2}\cdot\text{min}^{-1}$, and the sand transport rate at 30~40 cm is the largest. When the height is above 40 cm, the sand transport rate decreases gradually, and the height of 60~70 cm decreases to $0.0229 \text{ g}\cdot\text{cm}^{-2}\cdot\text{min}^{-1}$. Compared with the relative sand transport at different heights under different friction wind velocities, the sand transport at 0~40 cm height increases gradually with the increase of height from 10.61% to 26.07%, and the sand transport at 40~70 cm height decreases gradually from 17.03% to 3.95%. The boundary height is approximately 40 cm which increases with the increase of ridge height and ridge spacing. When the ridge height is 7.5 cm, the boundary height is 10~20 cm. When the ridge height is 10 cm, the boundary height increases from 10~20 cm at the ridge spacing of 5H to 20~30 cm at the ridge spacing of 15H. When the ridge height is 12.5 cm, the ridge spacing increases from 5H to 25H, the boundary height increases from 10~20 cm to 30~40 cm. When the ridge height increases to 15 cm, the boundary height increases from 30~40 cm at the ridge spacing of 15H

to 40~50 cm at the ridge spacing of 25H. The reason of the above changing is that, the influence of ridge on low-level drifting sand flux increases with the increase of ridge height, and its influence height also increases gradually. The influence mechanism of ridge spacing on the drifting sand flux structure is not clear for now.

3.3 Relationship between total sand transport rate and friction velocity

The total sand transport at 0~70 cm height was obtained by summing the sand transport of each layer, and then the total sand transport rate near the surface under different combinations of ridge height and spacing was calculated. The results show that under different ridge structures, the total sand transport rate increases with the increase of friction velocity, which conforms to the power function distribution, and the correlation of most ridge structures is higher than 0.9 (Fig. 5). With the increase of ridge spacing, the total sand transport rate increases rapidly, but the change of total sand transport rate with ridge height does not show a certain regularity. Compared with no ridges, the total sand transport rate under different ridge structures is lower when the friction velocity is $0.34 \text{ m}\cdot\text{s}^{-1}$ and $0.42 \text{ m}\cdot\text{s}^{-1}$. When the friction velocity increases to $0.51 \text{ m}\cdot\text{s}^{-1}$, the total sand transport rate of a few ridge structures with large ridge spacing increases rapidly, which has exceeded the total sand transport rate without ridge. When the friction velocity continues to increase, the total sand transport rate of all ridge structures at ridge spacing of 25H has exceeded that of no ridge.

This is because compared with the uniform bed with smooth surface, the take-off angle and saltation height of sand particles on the rough bed are significantly increased (Ding, 2010). When there is a ridge, the subducted sand particles rebound violently on the ridge, which not only increases the amount of sand transport in the upper airflow, but also the resistance to airflow decreases as the sand particles fly farther during the flight. The sand saltation height and horizontal distance are small on smooth bed surface. The sand particles are close to the ground in the transportation process, and the sand transport rate in the lower layer increases greatly, which increases the energy consumption of the airflow near the ground and weakens the transportation capacity of the airflow. Therefore, under a certain wind force, the sand transport rate on the loose bed surface with no ridges is smaller than that with ridge coverage. This phenomenon is also common on the Gobi surface covered with gravel (Zhang et al., 2007).

DISCUSSION

When there is no ridge, the sand transport rate decreases with the increase of height in a power function law. Under different ridge structures, the change of sand transport rate with height shows two trends. One is that the sand transport rate decreases exponentially with the increase of height. The other one shows an "elephant nose" effect, which is similar to the drifting sand flux structure in Gobi desert, as the near surface sand transport rate increases with the increase of height, and decreases exponentially above a certain height.

When the surface friction velocity exceeds the critical friction velocity of sand movement, the sand particles are separated from the surface and enter the airflow by the lifting power of wind. The movement of sand particles in drifting sand flux is very complex, which is not only affected by the airflow field, but also by the sand particle size, sand shape, environmental humidity and temperature (Neuman and Maljaars, 1997; Wiggs et al., 2004). Among them, the velocity of sand particles reflects the kinetic energy changes of airflow field and drifting sand flux in the process of sand movement, which has an important influence on sand transport process (Sharp, 1964; Zou et al., 2001). When the friction velocity is low, the surface wind pressure is also low, only a few sand particles leave the surface and begin to move, and the movement speed of sand particles is very slow. Because the average saltation velocity of sand particles is power function distribution with the saltation height (Zou et al., 2001; Dong et al., 2004; Yang et al., 2007), when the saltation height of sand particles is very low, the sand transport rate is small, and the percentage of sand transport in the lower layer is large. When the friction velocity increases, more sand particles leave the bed and begin to move. Because the resistance of sand particles in the movement process is small, they still have considerable momentum when they falling to the bed. Therefore, not only the falling sand particles themselves may rebound and continue to move, but also part of the sand particles around the falling point can splash into the motion state under its impact, and then cause a series of chain reactions. When the saltation motion state of sand particles in the drifting sand flux is stable, the amount of sand particles initiated by the direct effect of wind

can be ignored, and the sand particles in the drifting sand flux mainly taking off due to the impact collision effect (Anderson and Haff, 1991). Because the impact velocity of sand particles increases with the increase of friction velocity, the movement velocity and height of sand particles also increase with the increase of friction velocity. For the above reason, the larger the friction velocity, the larger the sand transport rate, the higher the proportion of sand transport in the higher height level. However, the sand movement mainly occurs in the limited height near the surface (Shao and Li, 1999; Kok and Renno, 2009), the proportion of sand transport in the near surface height layer is much larger than that in the higher height layer under different friction velocities.

Due to the influence of ridge, the wind velocity near surface decreases, the total sand transport decreases, the sand transport in the lower layer decreases as a whole, while the sand concentration in the upper layer changes relatively little, and the surface sand transport rate decreases exponentially with the increase of height. This is due to the variation of drifting sand flux structure caused by the influence of underlying surface (Ma, 1988). Taking a ridge height of 5 cm as an example, the drifting sand flux structure of five ridge spacings under different experimental wind velocities conforms exponential distribution, which can be expressed by the formula $q = A \exp(-Bh)$. Haas et al. (2004) pointed out in the study on the vertical distribution of surface sand transport rate of dunes in Tengger desert that the fitting coefficient A refers to the near surface sand transport, and B refers to the decreasing rate of surface sand transport rate with height. It can be seen that with the increase of wind velocity the value of A increases continuously, and the change of B value is not obvious. When the ridge spacing is $5H$, the friction velocity increases from $0.42 \text{ m}\cdot\text{s}^{-1}$ to $0.68 \text{ m}\cdot\text{s}^{-1}$, the value of A increases from 0.003 to 0.056, and the value of B first increases and then decreases. This shows that the sand transport rate increases continuously at height of $0\sim 10$ cm on the surface, and the decreasing rate of sand transport rate with height increases first and then decreases. When the friction velocity is $0.68 \text{ m}\cdot\text{s}^{-1}$, the ridge spacing increases from $5H$ to $25H$, the value of A increases from 0.056 to 6.696, and the value of B changes little. That is, when the ridge height is 5 cm, the sand transport rate at height of $0\sim 10$ cm increases with the increase of ridge spacing, and the decrease rate of sand transport rate among the five ridge spacings with height does not change significantly.

There are two reasons why the surface drifting sand flux structure covered by ridges has the "elephant nose" effect which is similar to that on Gobi surface. One reason is that, the sand transport in the low height layer is greatly affected by the ridge, especially for the structure of the last row ridge in the downwind direction which is close to the sand sampler. Due to the barrier action of ridges, the sand particles with low saltation height between ridges can not reach the end of the sample trough, so the sand transport in the low height layer mainly comes from the wind erosion of the bed surface behind the last row of ridges. With the increase of height, the mean diameter of wind erosion sediment decreases. Compared with coarse particles, fine particles have long transport distance and large transport height (Arens et al., 2002). Therefore, a large number of saltation fine particles from upwind ridges can reach the end of the sample trough, which increases the sand transport rate of the middle height layer of the sand sampler. The second reason is that, the collision properties between sand and ridge is different from that between sand and bare soil. Qu et al. (2005) considered that the "elephant nose" effect of the drifting sand flux structure on the Gobi surface is because the Gobi surface is mainly composed of gravel with large compactness, and the collision between moving particles and the surface is similar to elastic collision, resulting in large take-off angle and initial velocity of sand particles. When sand particles move to a higher space, they can make more use of the energy of high-level air flow, while the collision between sand particles and bare soil is opposite. Through field observation, Bagnold (1941) found that the maximum saltation height of sand particles can reach 2 m in gravel area, while the maximum saltation height of sand is 9 cm on the sandy surface. There is a certain similarity between the surface of ridge cover and the surface of Gobi. The ridge model is a rigid barrier, and the saltation particles are elastic collision when they collide with it. After the collision, the sand particles can rebound higher and farther, and make full use of the energy of the high-level air flow, resulting in the drifting sand flux mainly concentrated near the ridge height, which is similar to the "elephant nose" effect of the Gobi surface.

Compared with no ridges, the transport height of sand particles increased. Under most ridge structures, the

sand transport height reached a height layer of 60~70 cm. Since more than 90% of the saltation sand particles transport at height of 30 cm near the surface (Ding, 2010), the sand particles in the higher layer are mainly suspended. This also proves the conclusion of Fryear and Saleh (1993) that the variation of saltation sand transport with height follows a power function distribution law, while the suspension follows an exponential function distribution.

CONCLUSIONS

Using wind tunnel experiments, we measured the near-surface drifting sand flux structure and sand transport rate with different combinations of height and spacing for non-erodible ridges. The results show that: (1) Under the condition of no ridges, the sand transport rate at height of 0~70 cm above the sand bed decreases with the increase of height, but the decline rate between each height layer is becoming smaller and smaller. With the increase of friction velocity, the sand transport rate continues to increase, and the percentage of sand transported in the drifting sand flux layer near the bed surface decreases relatively, and the percentage of sand transport in the upper layer increases accordingly. More than 97% of the sand transport concentrate at height of 0~10 cm, the sand transport rate decreases with the increase of height in a power function. (2) Under ridge microtopography condition, the percentage of sand transport at height of 0~10 cm above the bed surface is significantly lower than that with no ridges. The sand transport rate at 0~70 cm height increases continuously with the increase of friction velocity, while the change of sand transport rate with height can be divided into two cases. One is that the sand transport rate decreases with the increase of height, and the fitting relationship between surface sand transport rate and height deviates from the power function law with no ridges, but mostly conforms the exponential function law of particle distribution of reaction saltation. The second one is that the sand transport rate increases with the increase of height below a certain height, and decreases with the increase of height above the certain height, showing the "elephant nose" effect similar to the drifting sand flux structure in Gobi desert. (3) The total sand transport rate at 0~70 cm height increases with the increase of friction velocity, which conforms to the power function distribution. With the increase of ridge spacing, the total sand transport rate increases rapidly, but the change of total sand transport rate with ridge height does not show a certain regularity. When the friction velocity is low, the total sand transport rate under different ridge structures is lower than that with no ridges, but when the friction velocity and ridge spacing are high, the total sand transport rate of some ridge structures exceeds that with no ridges.

ACKNOWLEDGMENTS

This study was supported by the National Natural Science Foundation of Hebei Province (No. D2019403168), the National Natural Science Foundation of China (Nos. 42101010, 41801007, 51909052, 42001380), the Social Science Foundation of Hebei province (No. HB21YJ014), the National Key R&D Program of China (No. 2020YFF0305905-06), the Science and Technology Planning Project of Hebei Academy of Sciences (No. 22103), the Fundamental Research Funds for the Universities in Hebei Province (Nos. QN2021028 and BJ2019045) and the S&T Program of Hebei (CN) (No. 19224205D).

DATA AVAILABILITY STATEMENT

The data that support the findings of this study are available from the corresponding author upon reasonable request.

REFERENCES

- Anderson, R. S., Haff, P. K. 1991. Wind modification and bed response during saltation of sand in air. *Acta Mechanica Supplementum*. 1: 21-51. DOI: 10.1007/978-3-7091-6706-9_2.
- Anderson, R. S., Hallet, B. 1986. Sediment transport by wind: Toward a general model. *Geological Society of America Bulletin*. 97(5): 523-525. DOI: 10.1130/0016-7606(1986)97%3C523:stbwta%3E2.0.co;2.
- Arens, S. M., Van Boxel, J. H., Abuodha, J. O. Z. 2002. Changes in grain size of sand in transport over a foredune. *Earth Surface Processes and Landforms*. 27(11): 1163-1175. DOI: 10.1002/esp.418.

- Avecilla, F., Panebianco, J. E., Buschiazzo, D. E. 2017. Meteorological conditions during dust (PM 10) emission from a tilled loam soil: Identifying variables and thresholds. *Agricultural and Forest Meteorology*, 244-245, 21-32. DOI: 10.1016/j.agrformet.2017.05.016.
- Bagnold, R. A. 1941. The Physics of Blown Sand and Desert Dunes. *The Geographical Journal*, 98(2)109. DOI: 10.2307/1787211.
- Butterfield, G. R. 1999, Application of thermal anemometry and high-frequency measurement of mass flux to aeolian sediment transport research. *Geomorphology*, 29(1-2): 31-58. DOI: 10.1016/s0169-555x(99)00005-7.
- Cheng, H., He, J. J., Zou, X. Y., et al. 2015. Characteristics of particle size for creeping and saltating sand grains in aeolian transport. *Sedimentology*, 62(5): 1497-1511. DOI: 10.1111/sed.12191.
- Ding, G. D. 2010. Aeolian physics. Beijing: China Forestry Publishing House. (in Chinese)
- Dong, Z., Liu, X., Wang, X., et al. 2004. Experimental investigation of the velocity of a sand cloud blowing over a sandy surface. *Earth Surface Processes and Landforms*. 29(3): 343-358. DOI: 10.1002/esp.1030.
- Favaro, E. A., Hugenholtz, C. H., Barchyn, T. E., et al. 2020. Wind regime, sediment transport, and landscape dynamics at a Mars analogue site in the Andes Mountains of Northwestern Argentina. *Icarus*, 113765. DOI: 10.1016/j.icarus.2020.113765.
- Frank, A. J., Kocurek, G. 1996. Airflow up the stoss slope of sand dunes: limitations of current understanding. *Geomorphology*, 17(1-3): 47-54. DOI: 10.1016/0169-555X(95)00094-L.
- Fryrear, D. W., Saleh, A. 1993. Field wind erosion: vertical distribution. *Soil Science*. 155: 294-300. DOI: 10.1097/00010694-199304000-00008.
- Ha, S. 2004. Preliminary study on the variation of surface aeolian sand flow structure on dunes in the southeast edge of Tengger Desert. *Chinese Science Bulletin*. 49(11): 1099-1104. (in Chinese)
- Horikawa, K., Hotta, S., Kubota, S. 1982. Experimental study of blown sand on wetted sand surface. *Coastal Engineering Japan*. 25(1): 177-195. DOI: 10.1080/05785634.1982.11924344.
- Huang, N., Zheng, X. J. 2007. Research history, achievements and trend on mechanism of aeolian transport. *Mechanics in Engineering*. 29(4): 9-16. (in Chinese)
- Jia, W. R., Zhang, C. L., Zou, X. Y., et al. 2019. Effects of ridge height and spacing on near-surface airflow field and wind erosion of a sandy soil: results of a wind tunnel study. *Soil & Tillage Research*. 186(3): 94-104. DOI: 10.1016/j.still.2018.10.005.
- Kok, J. F., Renno, N. O. 2009. A comprehensive numerical model of steady state saltation (COMSALT). *Journal of Geophysical Research Atmospheres*. 114(D17): 1-42. DOI: 10.1029/2009JD011702.
- Kok, J. F., Parteli, E. J. R., Michaels, T. I., et al. 2012. The physics of wind-blown sand and dust. *Reports on Progress in Physics*, 75(10), 106901. DOI: 10.1088/0034-4885/75/10/106901.
- Lancaster, N., Baas, A. 1998. Influence of vegetation cover on sand transport by wind: field studies at Owens Lake, California. *Earth Surface Processes & Landforms*. 23(1): 69-82. DOI: 10.1002/(SICI)1096-9837(199801)23:1<69::AID-ESP823>3.0.CO;2-G.
- Lancaster, N., Nickling, W. G., Neuman, M. K. et al. 1996. Sediment flux and airflow on the stoss slope of a barchan dune. *Geomorphology*, 17(3): 55-62. DOI: 10.1016/0169-555X(95)00095-M.
- Ma, S. W. 1987. Three laws of aeolian sand flow structure. *Inner Mongolia Forestry Science and Technology*. 3: 25-27. (in Chinese)
- Miao, C. Y., Yang, L., Chen, X. H., et al. 2012. The vegetation cover dynamics (1982–2006) in different erosion regions of the Yellow River basin, China. *Land Degradation & Development*, 23, 62–71. DOI: org/10.1002/ldr.1050.

Neuman, M. K., Maljaars, M. 1997. Wind tunnel measurement of boundary-layer response to sediment transport. *Boundary-Layer Meteorology*. 84(1): 67-83. DOI: 10.1023/a:1000349116747.

Qu, J. J., Huang, N., Ta, W. Q., et al. 2005. Structural characteristics of Gobi sand-drift and its significance. *Advances in Earth Sciences*. 20(1): 19-23. (in Chinese)

Shao, Y., Li, A. 1999. Numerical Modelling of Saltation in the Atmospheric Surface Layer. *Boundary-Layer Meteorology*. 91(2): 199-225. DOI: 10.1023/a:1001816013475.

Sharp, R. P. 1964. Wind-driven sand in Coachella Valley, California. *Geological Society of America Bulletin*. 71(5): 617-636. DOI: 10.1130/0016-7606(1964)75[785:WSICVC]2.0.CO;2.

Tsoar, H., White, B., Berman, E. 1996. The effect of slopes on sand transport-numerical modelling. *Landscape & Urban Planning*. 34(3-4): 171-181. DOI: 10.1016/0169-2046(95)00235-9.

Wiggs, G. F. S. 2001. Desert dune processes and dynamics. *Progress in Physical Geography*. 25(1): 53-79. DOI: 10.1191/030913301667883129.

Wu, Z. 2003. *Geomorphology of wind-drift sands and their controlled engineering*. Beijing: Science Press. (in Chinese)

Yang, P., Dong, Z., Qian, G., et al. 2007. Height profile of the mean velocity of an aeolian saltating cloud: Wind tunnel measurements by Particle Image Velocimetry. *Geomorphology*, 89(3): 320-334. DOI: 10.1016/j.geomorph.2006.12.012.

Zhang, K., Qu, J., Zu, R., et al. 2007. Characteristics of wind-blown sand on Gobi/mobile sand surface. *Geophysical Research Letters*. 54(2): 411-416. DOI: 10.1007/s00254-007-0827-2.

Zhang, Z. C., Zhang, Y., Pengfei Ma, P. F., et al. 2022. Aeolian sediment transport rates in the middle reaches of the Yarlung Zangbo River, Tibet Plateau. *Science of the Total Environment*, 826: 154238. DOI: 10.1016/j.scitotenv.2022.154238.

Zhao, C. N., Zhang, H. B., Wang, M., et al. 2021. Impacts of climate change on wind erosion in Southern Africa between 1991 and 2015. *Land Degradation & Development*, 32(6), 2169-2182. DOI: 10.1002/ldr.3895.

Zou, X. Y., Wang, Z. L., Hao, Q. Z., et al. 2001. The distribution of velocity and energy of saltating sand grains in a wind tunnel. *Geomorphology*, 36(3-4): 155-165. DOI: 10.1016/s0169-555x(00)00038-6.

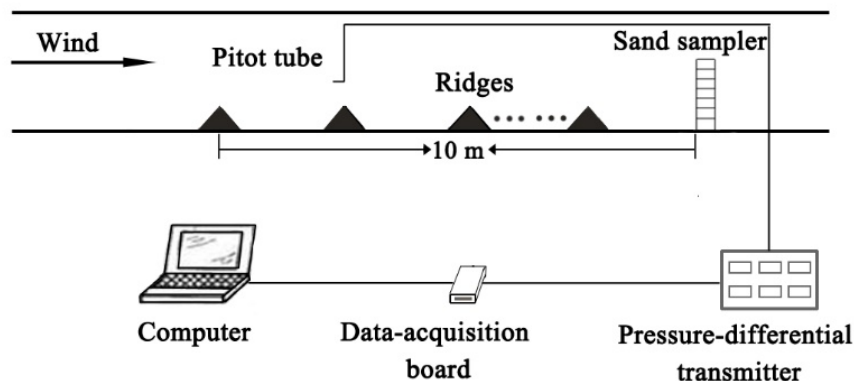


Fig. 1 Sketch of experimental equipments.



Fig. 2 Ridges arrangement in the wind erosion experiments. This figure shows ridge height is 10 cm and spacing is 10H (a) and one with no ridges condition (b).

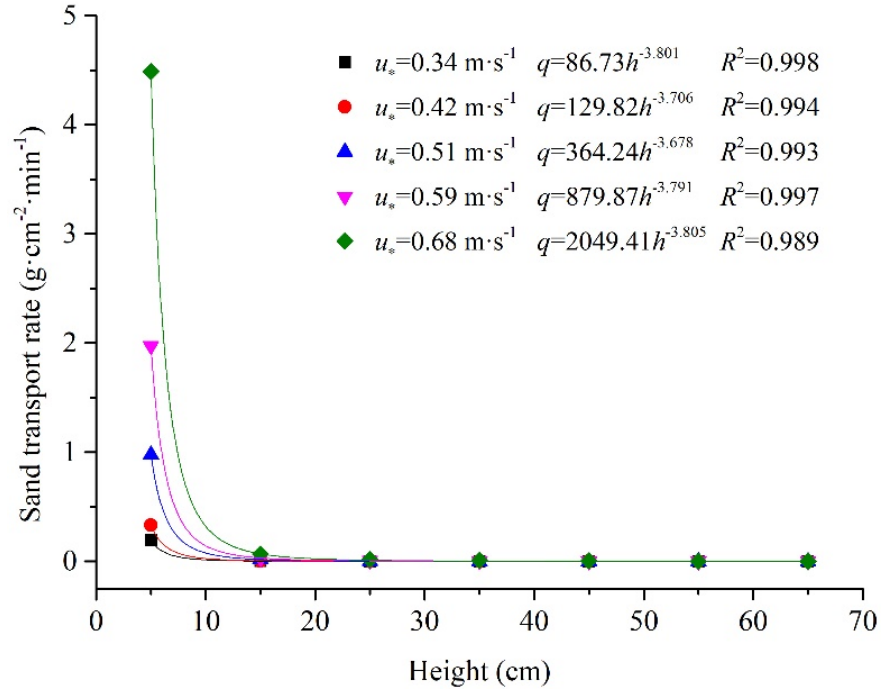


Fig. 3 Verticle distribution of sand flow above the bed surface with no ridges.

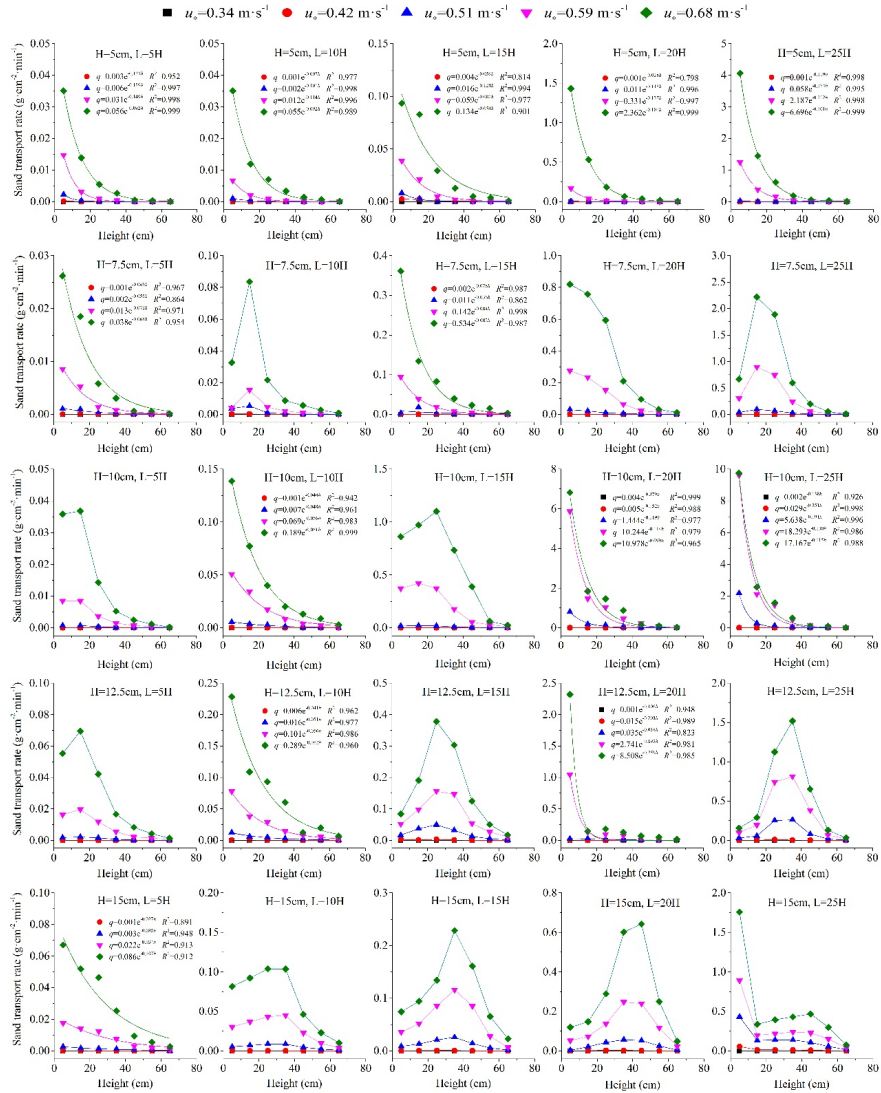


Fig. 4 Vorticity distribution of sand flow above the bed surface for different ridge structures.

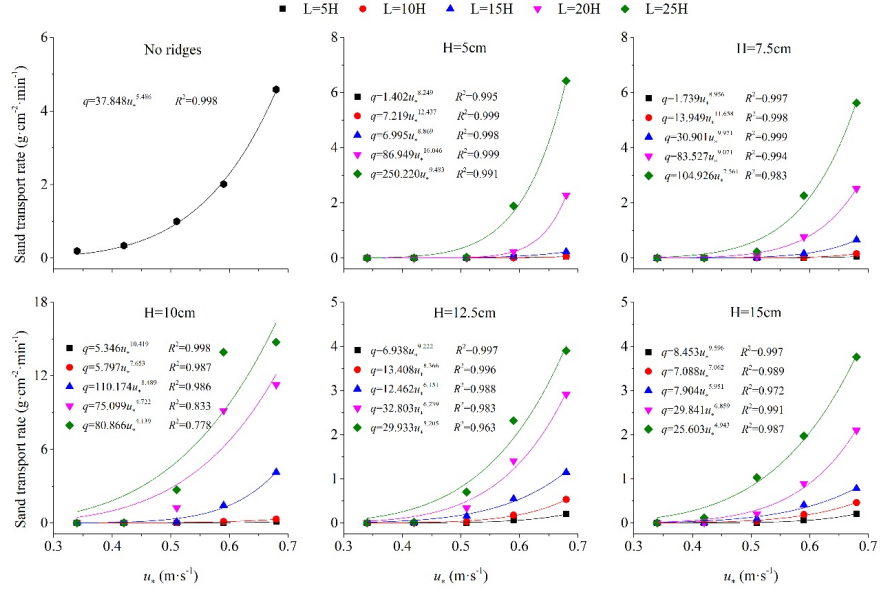


Fig. 5 Relationship between total sand transport rates near surface and friction velocities at different ridge spacing and height.

Table 1 Observation time in the wind erosion experiments (min).

Ridge spacing	Wind velocity $u_{70}(\text{m}\cdot\text{s}^{-1})$	Wind velocity $u_{70}(\text{m}\cdot\text{s}^{-1})$	Wind velocity $u_{70}(\text{m}\cdot\text{s}^{-1})$	Wind velocity $u_{70}(\text{m}\cdot\text{s}^{-1})$
	8	10	12	14
5H	15	15	6	5
10H	15	15	6	5
15H	15	15	6	2
20H	15	15	2	1
25H	15	15	2	1

Table 2 The percentage of sand transport at each height level above the bed surface with no ridges.

Friction velocity ($\text{m}\cdot\text{s}^{-1}$)	Height level (cm)				
	0~10	10~20	20~30	30~40	40~50
0.34	98.36	1.55	0.05	0.01	0.01
0.42	98.10	1.70	0.13	0.04	0.01
0.51	97.95	1.73	0.23	0.05	0.01
0.59	98.03	1.51	0.29	0.10	0.04
0.68	97.91	1.45	0.39	0.14	0.07

Table 3 The percentage of sand transport at each height layer as an example with ridge height of 5 cm.

Ridge spacing	Friction velocity (m·s ⁻¹)	Height layer (cm)						
5H		0~10	10~20	20~30	30~40	40~50	50~60	60~70
	0.34	33.33	16.67	16.67	16.67	16.67	0.00	0.00
	0.42	62.75	12.46	8.26	8.26	4.06	4.20	0.00
	0.51	80.11	11.42	3.40	2.25	1.11	0.57	1.15
	0.59	74.73	15.85	5.23	2.09	1.09	0.49	0.51
10H	0.68	60.54	23.96	9.43	4.62	0.90	0.51	0.04
	0.34	22.22	11.11	22.22	11.11	11.11	11.11	11.11
	0.42	61.74	22.35	10.61	0.00	5.30	0.00	0.00
	0.51	62.71	21.93	9.29	4.12	0.98	0.98	0.00
	0.59	65.95	19.30	8.56	3.70	1.54	0.77	0.18
15H	0.68	58.82	19.99	11.82	5.66	2.34	1.16	0.22
	0.34	85.71	3.57	3.57	3.57	3.57	0.00	0.00
	0.42	42.19	42.36	14.92	0.32	0.10	0.11	0.00
	0.51	72.60	23.49	2.33	0.87	0.28	0.15	0.29
	0.59	57.02	31.19	7.27	2.85	1.02	0.44	0.22
20H	0.68	40.93	36.28	12.94	5.60	2.22	1.61	0.42
	0.34	57.14	14.29	14.29	0.00	0.00	0.00	14.29
	0.42	12.45	54.56	18.87	7.14	2.38	2.38	2.22
	0.51	66.48	19.00	8.92	3.36	1.68	0.56	0.00
	0.59	70.98	16.87	5.82	3.34	1.90	0.80	0.29
25H	0.68	62.82	23.32	8.12	2.91	1.73	0.76	0.35
	0.34	33.33	16.67	16.67	16.67	0.00	0.00	16.67
	0.42	67.40	19.24	7.67	2.53	1.29	1.29	0.60
	0.51	78.02	12.28	5.73	2.54	0.96	0.32	0.15
	0.59	66.38	20.32	8.75	2.35	1.44	0.55	0.21
	0.68	63.24	22.54	9.52	2.95	0.87	0.69	0.19

Supplemental Table 1 The percentage of sand transport at each height layer with ridge height of 7.5 cm.

Ridge spacing	Friction velocity (m·s ⁻¹)	Height layer (cm)						
5H		0~10	10~20	20~30	30~40	40~50	50~60	60~70
	0.34	33.33	0.00	0.00	33.33	0.00	33.33	0.00
	0.42	38.95	25.28	14.04	5.24	8.43	5.24	2.81
	0.51	41.07	38.46	9.95	5.92	2.65	1.28	0.66
	0.59	52.03	31.97	8.50	4.73	1.69	0.84	0.24
10H	0.68	47.71	33.71	10.61	5.56	1.18	1.01	0.23
	0.34	40.00	33.33	6.67	6.67	13.33	0.00	0.00
	0.42	46.52	44.79	5.26	1.29	1.26	0.44	0.44
	0.51	35.00	50.17	9.85	3.12	1.08	0.47	0.31
	0.59	15.07	55.33	16.53	7.62	3.44	1.58	0.43
15H	0.68	20.94	53.61	13.94	5.56	3.63	1.79	0.53
	0.34	50.00	20.00	10.00	20.00	0.00	0.00	0.00
	0.42	52.87	20.76	11.34	7.39	3.82	1.91	1.91
	0.51	12.95	76.85	5.95	2.47	1.28	0.35	0.14
	0.59	56.26	23.13	11.08	5.03	2.77	1.40	0.33

Ridge spacing	Friction velocity (m·s ⁻¹)	Height layer (cm)						
20H	0.68	54.73	20.30	12.57	6.03	3.53	2.31	0.53
	0.34	36.36	18.18	9.09	9.09	18.18	9.09	0.00
	0.42	45.33	28.50	13.72	6.29	4.10	2.05	0.00
	0.51	43.41	30.43	15.11	6.96	2.85	0.88	0.37
	0.59	35.87	30.49	19.98	8.44	2.95	1.63	0.64
25H	0.68	32.56	30.07	23.59	8.33	3.75	1.22	0.48
	0.34	24.00	32.00	12.00	4.00	4.00	12.00	12.00
	0.42	35.47	48.68	11.81	2.16	0.58	0.55	0.75
	0.51	16.10	40.75	28.98	10.55	2.76	0.67	0.19
	0.59	13.41	39.64	32.79	10.52	2.55	0.85	0.25
	0.68	11.85	39.44	33.56	10.58	3.46	0.92	0.19

Supplemental Table 2 The percentage of sand transport at each height layer with ridge height of 10 cm.

Ridge spacing	Friction velocity (m·s ⁻¹)	Height layer (cm)						
5H		0~10	10~20	20~30	30~40	40~50	50~60	60~70
	0.34	36.36	27.27	18.18	9.09	0.00	9.09	0.00
	0.42	25.91	20.80	15.69	16.06	5.47	5.11	10.95
	0.51	35.43	34.69	16.53	7.07	3.96	1.53	0.79
	0.59	36.68	36.61	15.53	6.29	3.11	1.37	0.42
10H	0.68	37.31	38.33	14.88	5.47	2.54	1.24	0.24
	0.34	50.00	20.00	20.00	10.00	0.00	0.00	0.00
	0.42	33.61	27.56	20.00	8.74	5.04	2.52	2.52
	0.51	39.11	27.28	19.98	8.01	3.23	1.68	0.72
	0.59	43.22	29.36	14.58	6.92	3.34	1.89	0.68
15H	0.68	46.17	25.73	13.31	6.68	4.33	2.89	0.89
	0.34	20.83	16.67	16.67	8.33	8.33	12.50	16.67
	0.42	22.84	30.56	27.27	12.54	4.31	1.54	0.95
	0.51	25.30	29.18	25.71	12.38	5.30	1.75	0.37
	0.59	25.91	29.31	25.94	12.33	3.72	2.06	0.73
20H	0.68	20.78	23.45	26.57	17.73	9.38	1.49	0.60
	0.34	95.74	2.13	1.06	0.00	1.06	0.00	0.00
	0.42	72.30	13.18	8.04	4.03	1.55	0.67	0.22
	0.51	65.42	15.27	11.41	5.03	1.80	0.84	0.24
	0.59	64.00	16.04	11.19	4.95	2.64	0.90	0.28
25H	0.68	60.43	16.36	12.93	7.75	1.48	0.80	0.24
	0.34	59.26	11.11	7.41	7.41	7.41	3.70	3.70
	0.42	87.46	6.62	3.41	1.36	0.54	0.34	0.27
	0.51	80.40	10.82	5.13	2.02	1.13	0.38	0.11
	0.59	68.95	15.23	10.23	3.59	1.20	0.62	0.18
	0.68	66.07	17.46	10.70	4.19	0.77	0.63	0.19

Supplemental Table 3 The percentage of sand transport at each height layer with ridge height of 12.5 cm.

Ridge spacing	Friction velocity (m·s ⁻¹)	Height layer (cm)						
5H		0~10	10~20	20~30	30~40	40~50	50~60	60~70
	0.34	25.00	50.00	0.00	25.00	0.00	0.00	0.00
	0.42	32.21	31.97	21.63	14.18	0.00	0.00	0.00
	0.51	25.36	31.87	23.93	10.86	4.11	2.66	1.21
	0.59	28.32	34.19	20.43	9.52	3.86	2.54	1.15
10H	0.68	28.02	35.18	21.33	8.42	4.22	2.13	0.70
	0.34	27.27	18.18	9.09	9.09	9.09	18.18	9.09
	0.42	36.55	20.01	17.85	12.62	7.82	3.43	1.72
	0.51	42.36	20.98	17.65	9.57	5.10	3.03	1.31
	0.59	44.44	21.81	16.51	8.22	4.55	3.19	1.27
15H	0.68	43.10	20.54	17.60	11.38	2.37	3.74	1.27
	0.34	9.09	27.27	45.45	9.09	0.00	9.09	0.00
	0.42	29.69	16.42	34.98	13.67	3.66	1.03	0.55
	0.51	10.57	23.90	31.97	20.92	8.13	3.39	1.12
	0.59	9.48	17.97	28.71	26.98	9.87	4.92	2.07
20H	0.68	7.32	16.63	32.95	26.38	10.85	4.39	1.48
	0.34	60.00	15.00	10.00	10.00	5.00	0.00	0.00
	0.42	77.16	8.75	5.71	3.80	2.19	1.91	0.48
	0.51	7.27	83.89	4.24	2.39	1.36	0.58	0.27
	0.59	74.27	8.85	6.85	5.26	2.81	1.42	0.54
25H	0.68	79.73	5.00	6.19	4.44	2.36	1.71	0.57
	0.34	14.29	25.71	40.00	11.43	8.57	0.00	0.00
	0.42	7.54	17.10	43.18	24.15	6.16	1.55	0.33
	0.51	4.21	8.14	35.99	37.30	11.36	2.53	0.48
	0.59	4.26	8.40	32.01	35.10	16.48	2.87	0.88
	0.68	4.01	7.45	28.79	38.94	16.70	3.30	0.82

Supplemental Table 4 The percentage of sand transport at each height layer with ridge height of 15 cm.

Ridge spacing	Friction velocity (m·s ⁻¹)	Height layer (cm)						
5H		0~10	10~20	20~30	30~40	40~50	50~60	60~70
	0.34	0.00	0.00	33.33	0.00	33.33	0.00	33.33
	0.42	27.70	18.47	21.02	14.51	9.15	5.28	3.87
	0.51	4.59	29.53	27.79	19.78	9.16	6.31	2.85
	0.59	30.66	24.61	21.54	13.26	5.21	3.37	1.35
10H	0.68	32.22	24.90	22.29	12.17	4.54	2.63	1.25
	0.34	15.38	23.08	15.38	15.38	15.38	7.69	7.69
	0.42	15.14	18.79	22.51	19.28	12.83	7.80	3.65
	0.51	14.49	18.76	23.16	22.81	12.20	6.08	2.51
	0.59	15.86	19.19	22.53	23.49	11.85	5.06	2.03
15H	0.68	17.72	20.02	22.54	22.49	10.03	4.99	2.22
	0.34	14.29	14.29	19.05	19.05	14.29	9.52	9.52
	0.42	10.83	16.09	25.01	24.84	13.81	5.94	3.48
	0.51	9.70	14.51	23.19	28.78	15.60	6.07	2.16
	0.59	8.74	12.73	20.90	28.40	20.83	6.73	1.66

Ridge spacing	Friction velocity (m·s ⁻¹)	Height layer (cm)						
20H	0.68	9.52	12.05	17.18	29.28	20.63	8.40	2.94
	0.34	14.29	14.29	28.57	21.43	7.14	7.14	7.14
	0.42	7.86	13.81	25.81	28.88	15.73	6.06	1.86
	0.51	1.57	10.06	21.01	27.64	25.34	12.04	2.34
	0.59	5.91	8.18	15.49	27.82	26.89	13.15	2.56
	0.68	5.71	7.04	13.79	28.65	30.62	11.88	2.32
25H	0.34	61.90	14.29	9.52	9.52	4.76	0.00	0.00
	0.42	49.27	13.95	12.55	10.90	7.51	4.26	1.58
	0.51	41.98	12.87	13.76	13.56	10.62	5.58	1.63
	0.59	45.30	10.13	11.07	12.21	11.57	7.62	2.11
	0.68	46.69	8.98	10.47	11.47	12.45	7.92	2.02